Appl. Phys. B 90, 489–496 (2008)
DOI: 10.1007/s00340-007-2911-4

**Applied Physics B**
**Lasers and Optics**

S. MANIVANNAN[1]
S. DHANUSKODI[1,✉]
S.K. TIWARI[2]
J. PHILIP[3]

# Laser induced surface damage, thermal transport and microhardness studies on certain organic and semiorganic nonlinear optical crystals

[1] School of Physics, Bharathidasan University, Tiruchirappalli 620024, India
[2] Laser Physics Applications Division, Raja Ramanna Centre for Advanced Technology, Indore 452013, India
[3] Department of Instrumentation, Cochin University of Science and Technology, Cochin 682022, India

**Received: 6 June 2007 / Revised version: 28 September 2007**
**Published online: 22 January 2008 •** 

**ABSTRACT** *N*-alkyl-2,6-dimethyl-4(1H)-pyridinones, salts of 4-dimethylaminopyridine and 2-amino-5-nitropyridine are considered to be potential candidates for nonlinear optical (NLO) applications, in particular for the generation of blue-green laser radiation. Single crystals were grown following the slow evaporation technique at constant temperature. Single-shot laser-induced surface damage thresholds in the range 3–10 GW/cm$^2$ were measured using a 18 ns Q-switched Nd:YAG laser. The surface morphologies of the damaged crystals were examined under an optical microscope and the nature of damage identified. The Vicker's microhardness was determined at a load of 98.07 mN. The thermal transport properties, thermal diffusivity ($\alpha$), thermal effusivity ($e$), thermal conductivity ($K$) and heat capacity ($C_p$), of the grown crystals were measured by an improved photopyroelectric technique at room temperature. All the results are presented and discussed.

**PACS** 42.70.Mp; 61.66.Hq; 67.80.Gb; 42.65.-k

## 1 Introduction

Organic materials are emerging as an alternative to inorganic materials because of their efficient molecular nonlinearity over a broad frequency range, low cost, low dielectric constant, inherent synthetic flexibility, high optical damage threshold, ultrafast response with better processability, ease of fabrication and integration into devices [1–3]. In optical signal processing, femtosecond ($10^{-15}$) response time is needed and this is achieved by organic materials. The laser damage threshold for organic polymeric materials is greater than 10 GW/cm$^2$ with picosecond pulses. The dielectric constant of organic materials is lower than those of inorganic crystals and thus leads to the minimization of phase mismatch [4–6]. Similarly, in many respects, the semiorganic L-arginine phosphate monohydrate (LAP) crystal can match the inorganic potassium dihydrogen orthophosphate (KDP). LAP possesses a large nonlinear optical (NLO) coefficient, $d_{21} = 2.14d_{36}$ (KDP) and is characterized by an extremely high laser damage threshold. It has been explored as material in ultrafast pulse and strong laser doubling techniques. The deuterated form of LAP (DLAP) has a higher damage threshold for Nd:YAG laser light than LAP [7]. Likewise, the first reported complex type semiorganic NLO material is bisthiourea cadmium chloride (BTCC). It belongs to the $Pmn2_1$ space group; transparent from 300 nm to 1450 nm and has a NLO coefficient $d_{11} = 2.75d_{36}$ (KDP). Along the phase matching direction, its second harmonic generation (SHG) efficiency is almost the same as that of urea [8]. The compound with the largest first order hyperpolarizability ($\beta$) value to date is 3-methyl-4-methoxy-4′-nitrostilbene (MMONS) [9], which exhibits a powder SHG efficiency 3000 times that of the KDP. Jiang and Fang have grown high quality crystals of 3-methoxy-4-hydroxy benzaldehyde (MHBA), which can be used to generate blue laser light by frequency doubling a GaAlAs laser-diode [10]. Although this crystal does not belong to the ranks of a few well-known organic crystals with the highest SHG efficiency, its transparency is excellent with a UV cutoff wavelength of 370 nm. Thus, MHBA is a good candidate for a blue light generator by frequency doubling IR diode laser light. MHBA crystallizes in the $P2_1$ space group and its effective NLO coefficient ($d_{\text{eff}}$) is 8.47 pm/V at 1064 nm (Nd:YAG) and 10 pm/V at 830 nm (Ti:$Al_2O_3$). Blue light of 405.5 nm ($\sim 3\,\mu$W) has been obtained from MHBA by doubling of 809 nm input laser (1 W). They have also prepared and characterized thin-film waveguides for MHBA with dimensions of upto 10 mm × 10 mm [11].

In line of these materials, *N*-alkyl-2,6-dimethyl-4(1H)-pyridinones, salts of 4-dimethylaminopyridine and 2-amino-5-nitropyridine are considered to be potential candidates for NLO applications, in particular for the generation of blue-green laser radiations by frequency doubling [12–14]. For example, the organic 4-dimethylaminopyridinium L-tartrate dihydrate (DMAPT · 2 $H_2O$) and semiorganic 2-amino-5-nitropyridinium tetrafluoroborate (2A5NPFB) salts show 1.13 and 40 times greater SHG efficiencies respectively than the KDP in the pulverized form with a very good optical transmittance in the visible and near infrared regions [13, 14]. Laser induced damage is a catastrophic complex phenomenon, which is one of the important device related properties of NLO crystals. This involves the interaction of high power laser radiation with matter, followed by various physical, chemical, optical, thermal and other processes in the

✉ Fax: +91-431-2407045, E-mail: dhanus2k3@yahoo.com

material. It is well known that the harmonic conversion efficiency is proportional to the power density of the fundamental beam. One of the convenient ways to increase the efficiency is to focus the beam into the crystal. However, this often leads to damage of the crystal and so it is useful to prescribe the maximum permissible power for a particular crystal. The surface of a material often tends to get damaged at power levels an order of magnitude lower than that for the bulk. On the other hand, the single shot surface damage threshold is the limiting parameter for crystals, which are useful in high average power harmonic generation such as LAP and KDP [15].

Another important property of any crystal for device applications is its mechanical strength represented by its hardness. The indentation hardness is measured as the ratio of applied load to the area of the indentation [16, 17]. In addition to these, the thermal properties of crystals are of basic importance, which are relevant for various applications. When a laser beam passes through the crystal, part of the light will be absorbed by the crystal and converted into heat, so a temperature gradient is formed and a corresponding thermal expansion occurs. If the thermal expansion coefficients of the crystal are anisotropic, the crystal will crack when it absorbs a high enough thermal energy. A crystal with a high specific heat will have a lower temperature gradient than a crystal with a low specific heat, while absorbing the same quantity of heat. Therefore, in the former case the crystal is not easily destroyed by the temperature gradient [18]. In light of the above considerations, systematic investigations have been carried out on selected NLO crystals as listed below.

The crystals chosen for the present investigations are the following: 1-ethyl-2,6-dimethyl-4(1H)-pyridinone trihydrate (EDMP · 3 $H_2O$) [19], 1-methyl-2,6-dimethyl-4(1H)-pyridinone trihydrate (MDMP · 3 $H_2O$) [20], 3-[(1E)-*N*-ethylethanimidoyl]-4-hydroxy-6-methyl-2H-pyran-2-one (EMPO) [21], bis-2,7-diethylaminohepta-2,5-dien-4-one (BEDO) [22], 1-ethyl-2,6-dimethyl-4-hydroxypyridinium chloride dihydrate (EDMPCl · 2 $H_2O$) , 1-ethyl-2,6-dimethyl-4-hydroxypyridinium bromide dihydrate (EDMPBr · 2 $H_2O$) [23], 1-methyl-2,6-dimethyl-4-hydroxypyridinium chloride monohydrate (MDMPCl · $H_2O$), 1-methyl-2,6-dimethyl-4-hydroxypyridinium bromide monohydrate (MDMPBr · $H_2O$), 4-dimethylaminopyridinium dihydrogen phosphate (DMAPDP) [24, 25], 4-dimethylaminopyridinium chloride dihydrate (DMAPCl · 2 $H_2O$), DMAPT · 2 $H_2O$ [13], 2A5NPFB [14] and 2-amino-5-nitropyridinium fluoride (2A5NPF). The crystals chosen in this work are all pyridine based organic and semiorganic potential NLO crystals having different donors and acceptors in the respective compounds. In this paper, we report the result of measurement of the single shot laser induced surface damage threshold and Vicker's micro hardness of the grown crystals. The thermal transport properties, namely thermal diffusivity ($\alpha$), thermal effusivity ($e$), thermal conductivity ($K$) and heat capacity ($C_p$) of EMPO, BEDO, EDMP · 3 $H_2O$, MDMP · 3 $H_2O$ and DMAPDP single crystals are measured using an improved photopyroelectric (PPE) technique. The experimental details, results obtained and a discussion of the results are given in the following sections.

## 2 Experimental methods

All the single crystals used in the present investigation were grown by the slow evaporation technique at constant temperature. The detailed procedure of material synthesis, the conditions for single crystal growth, and the structural, thermal and optical properties of the grown crystals have already been reported [13, 14, 19–25]. In order to determine the laser induced surface damage threshold, a Q-switched Nd: YAG laser (Raja Ramanna Centre for Advanced Technology, India) (1064 nm, 18 ns, 1.0 Hz) was used (Fig. 1). The laser beam was focused using a focusing lens (focal length 500 mm) and the measured focal spot size was nearly 123 μm ($1/e^2$ radius). The combination of a polarizer and transmission filters serves to adjust the input intensity to the required level and the measurement was carried out at phase matching condi-

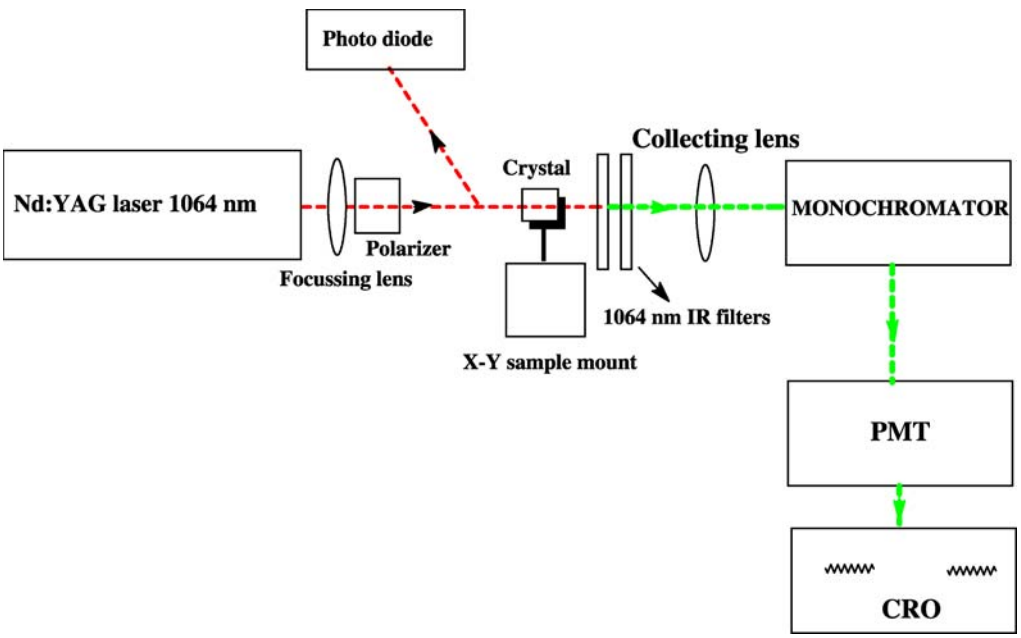


**FIGURE 1** Experimental set up for laser induced surface damage threshold measurement

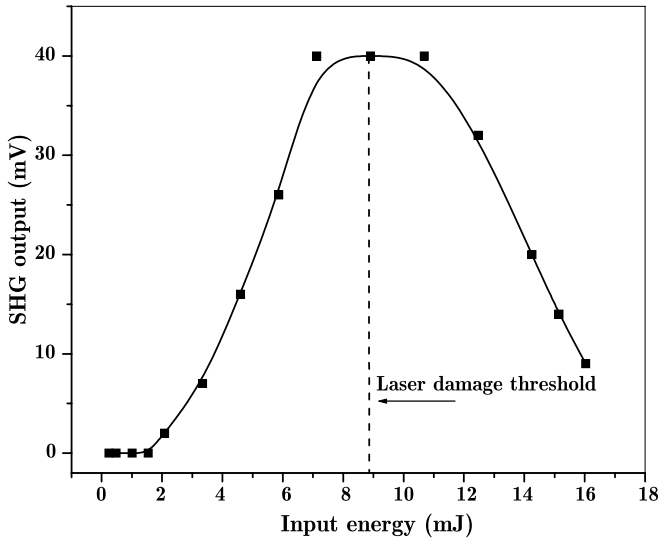


**FIGURE 2** Laser induced surface damage threshold of MDMP · 3 $H_2O$

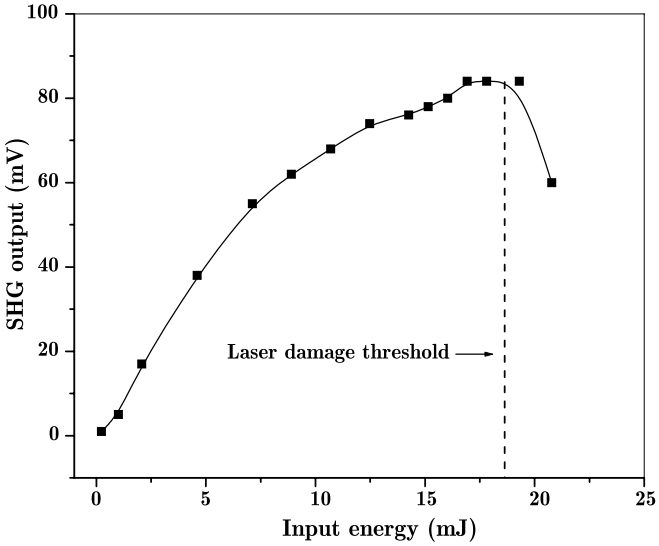


**FIGURE 4** Laser induced surface damage threshold of DMAPT · 2 $H_2O$

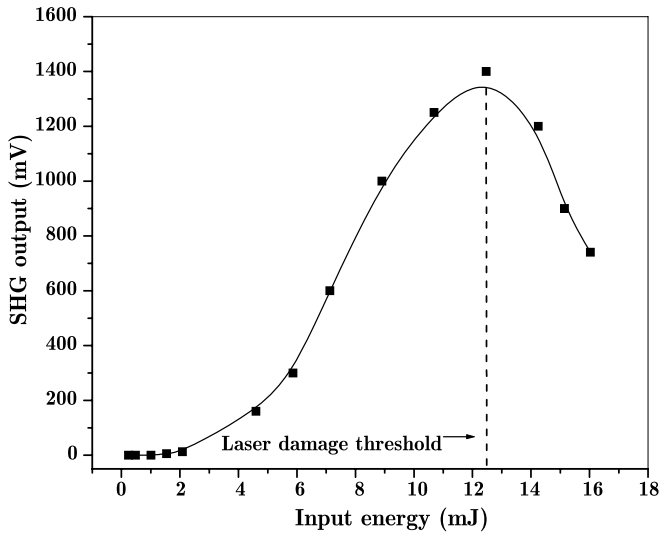


**FIGURE 3** Laser induced surface damage threshold of EDMP · 3 $H_2O$

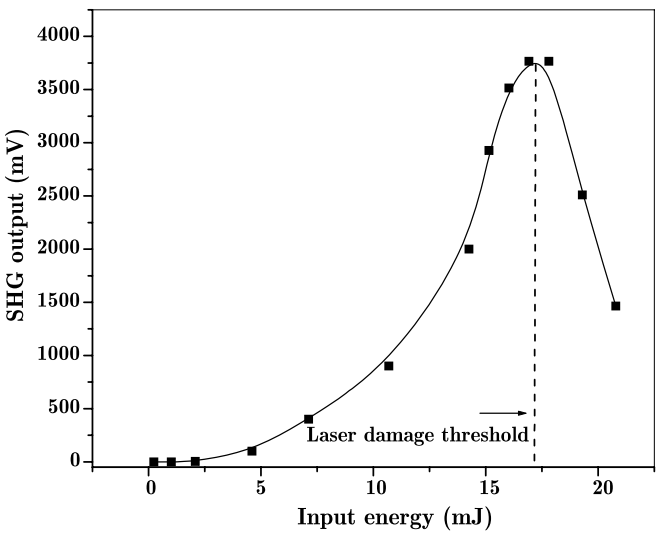


**FIGURE 5** Laser induced surface damage threshold of 2A5NPFB

tions. A photo diode was used to identify the pulse-to-pulse variation of the incident beam and sufficient time was allowed to stabilize the output power of the laser. The crystals were placed on a $X$–$Y$ translator and kept slightly away from the focal spot of the beam to avoid any possible damage. The scattered second harmonic signal from the crystal was collected using a collection lens and was monitored using a monochromator, photomultiplier tube (PMT) and cathode ray oscilloscope (CRO). The occurrence of damage was monitored on the CRO and irrespective of whether the damage had occurred or not the sample was moved to a new site. The separation between the two sites was kept at least five times the spot size on the crystal surface. Thus, any kind of cumulative effect was completely avoided. This facilitated accurate measurement, eliminating the possibility of the sample getting damaged at lesser radiation fluence [26, 27]. Upto ten samples of each crystal were used in this measurement. Based on the number of observations, the mean surface damage threshold of the grown crystals were calculated by plotting the second harmonic generation (SHG) output (mV) against the energy (mJ) of the input beam (Figs. 2–5). It is known that the SHG output is increased on increasing the incident energy and reaches a maximum until damage occurs and decreases after damage for further increases of incident energy. The corresponding energy for maximum SHG output was taken for calculation. Thus, the surface damage threshold of the crystals was calculated using the expression

$$\text{Power density}\,(P) = E/\tau\pi r^2\,, \tag{1}$$

where $E$ is the energy (mJ), $\tau$ is the pulse width (ns) and $r$ is the radius of the spot (mm). In order to probe the nature of damage in the crystals investigated, the damaged samples were subsequently examined under an optical microscope. The Vicker's microhardness (Hv) was evaluated using a Shimadzu HMV-2T microhardness tester. Indentation was carried out using a Vicker's indenter at a constant load of 98.07 mN. The indentation time was kept constant at 15 s. Several indentations were made and the average value was used to calculate the microhardness.

An improved photopyroelectric (PPE) technique is used to determine the thermal transport properties of the crystals. Since none of the investigated materials showed any kind of phase transition before melting/decomposition in DSC analysis (Mettler Toledo DSC822$^e$) performed in the temperature range 30–500 °C, all the measurements were carried out at room temperature only. A detailed description of the experimental set up and the determination of the thermal parameters of crystals by this technique has been reported elsewhere [25, 28]. In order to get good uniform surface finish, each crystal having thickness of $< 1$ mm was carefully polished using a polishing sheet. To enhance its optical absorption, a very thin layer of carbon black from a benzene flame was carefully coated onto the illuminated surface of the prepared samples to be illuminated. In this measurement, a thermally thick, polyvinylidene diflouride (PVDF) film with a thickness of 28 mm, coated with Ni-Cr on both sides, with a pyroelectric coefficient $P = 0.25 \times 10^{-8}\,\mathrm{V\,cm^{-1}K^{-1}}$ was used as the pyroelectric detector. The thermally thick pyroelectric detector film was attached to one side of the sample, which is also thermally thick, and the combination is mounted on a thermally thick backing medium made up of copper. The other side of the sample was illuminated by an intensity modulated beam of light, which gives rise to periodic temperature variations by optical absorption. The thermal waves so generated propagate through the sample and are detected by the pyroelectric detector. A 120 mW He-Cd laser of wavelength 442 nm, intensity modulated by a mechanical chopper, has been used as the optical heating source. The sample-detector-backing assembly was enclosed in a chamber, and was kept at room temperature (28 °C). The signal output was measured with a lock-in amplifier (Stanford Research Systems-Model: SR830 DSP) having 10 MΩ input impedance and 50 pF input capacitance. The frequency of the modulation of the laser source was kept in the range 65–75 Hz to ensure that the detector, the sample and the backing medium are thermally thick during measurements. The thermal thickness of each samples in this experiment have been selected by plotting the PPE amplitude and phase with frequency at room temperature. Thus, the measurement of the PPE signal phase and amplitude enables one to determine the thermal diffusivity ($\alpha$) and thermal effusivity ($e$). From the measured values of $\alpha$ and $e$; thermal conductivity ($K$) and heat capacity ($C_p$) were calculated.

## 3 Results and discussion

The damage threshold energy is calculated by plotting the SHG intensity against incident energy for each sample (Figs. 2–5). The laser damage thresholds for other crystals in the same family that do not exhibit second order NLO prop-

| Crystal | Laser induced surface damage ($GW/cm^2$) | Test parameters (laser wavelength, pulse width, pulse frequency, spot diameter) |
|---|---|---|
| EMPO | 7.50 | 1064 nm, 18 ns, 1.0 Hz, 123 μm |
| BEDO | 7.29 | 1064 nm, 18 ns, 1.0 Hz, 123 μm |
| $EDMP \cdot 3H_2O$ | 7.60 | 1064 nm, 18 ns, 1.0 Hz, 123 μm |
| $MDMP \cdot 3H_2O$ | 5.28 | 1064 nm, 18 ns, 1.0 Hz, 123 μm |
| $EDMPCl \cdot 2H_2O$ | 3.40 | 1064 nm, 18 ns, 1.0 Hz, 123 μm |
| $EDMPBr \cdot 2H_2O$ | 6.36 | 1064 nm, 18 ns, 1.0 Hz, 123 μm |
| $MDMPCl \cdot H_2O$ | 3.55 | 1064 nm, 18 ns, 1.0 Hz, 123 μm |
| $MDMPBr \cdot H_2O$ | 7.69 | 1064 nm, 18 ns, 1.0 Hz, 123 μm |
| DMAPDP | 4.80 | 1064 nm, 18 ns, 1.0 Hz, 123 μm |
| $DMAPCl \cdot 2H_2O$ | 5.62 | 1064 nm, 18 ns, 1.0 Hz, 123 μm |
| $DMAPT \cdot 2H_2O$ | 9.72 | 1064 nm, 18 ns, 1.0 Hz, 123 μm |
| 2A5NPFB | 7.48 | 1064 nm, 18 ns, 1.0 Hz, 123 μm |
| 2A5NPF | 7.98 | 1064 nm, 18 ns, 1.0 Hz, 123 μm |
| Literature [29-31] | | |
| KDP | 14.4 | 1064 nm, 12 ns, 30 μn |
| Ammonium dihydrogen phosphate (ADP) | 6.4 | 1064 nm, 12 ns, 30 μm |
| Potassium niobate (KN) | 0.15–0.18 | 1064 nm, 25 ns |
| Lithium tantalate (LT) | 0.47 | 1064 nm, 30 ns |
| Gallium arsenide (GaAs) | 0.05 | 1064 nm, 45 ns |
| Beta-barium borate (BBO) | 2.6 | 1064 nm, 10 ns, 10 Hz |
| Lithium triborate (LBO) | > 0.6 | 1064 nm, 18 ns, 10 Hz |
| Lithium niobate (LN) | 11.1 | 1064 nm, 12 ns, 30 μm |
| Potassium titanyl phosphate (KTP) | 1.5–2.2 | 1064 nm, 11 ns, 2 Hz |
| Silver thiogallate (AGS) | 0.01 | 1064 nm, 20 ns, 10 Hz |
| Silver gallium selenide (AGSe) | 0.013–0.04 | 1064 nm, 23 ns |
| Lithium lodate (LI) | 3.2 | 1064 nm, 12 ns, 30 μm |
| Cesium lithium borate (CLBO) | 2.9 | 266 nm, 8 ns |
| Potassium pentaborate tetrahydrate (KB5) | > 0.085 | 1064 nm, 12 ns, 10 Hz |
| Deuterated L-arginine phosphate monohydrate (DLAP) | 9–13 | 1064 nm, 1 ns |
| LAP | 10–13 | 1064 nm, 1 ns |
| MHBA | 2 | 1064 nm, 10 ns |
| 3-Methyl-4-nitropyridine-1-oxide (POM) | 10.5 | 1064 nm, 20 ns |
| 2-cyclooctylamino-5-nitropyridine (COANP) | > 0.0015 | 1064 nm, 250 ns |
| *N*-(4-nitrophenyl)-L-prolinol (NPP) | 10 | 622 nm, 0.0001 ns |
| L-pyrrolidone-2-carboxylic acid (L-PCA) | 17 | 1064 nm, 20 ns |

**TABLE 1** Laser induced surface damage threshold of the grown crystals

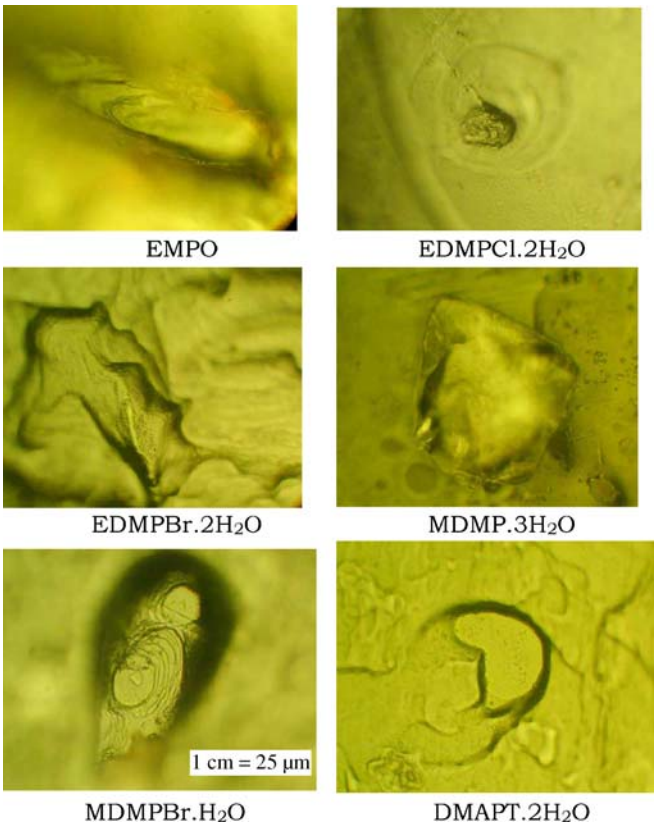


**FIGURE 6** Optical micrograph of laser induced damage (400 ×) viewed along the axis of the laser radiation

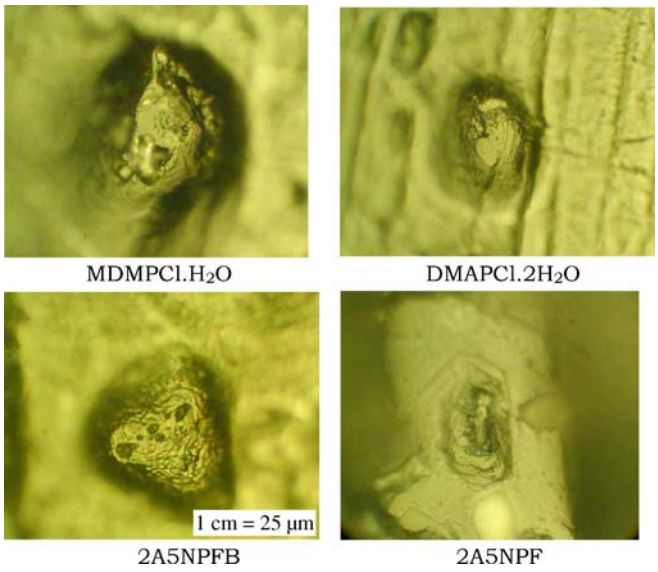


**FIGURE 7** Optical micrograph of laser induced damage (400 ×) viewed along the axis of the laser radiation

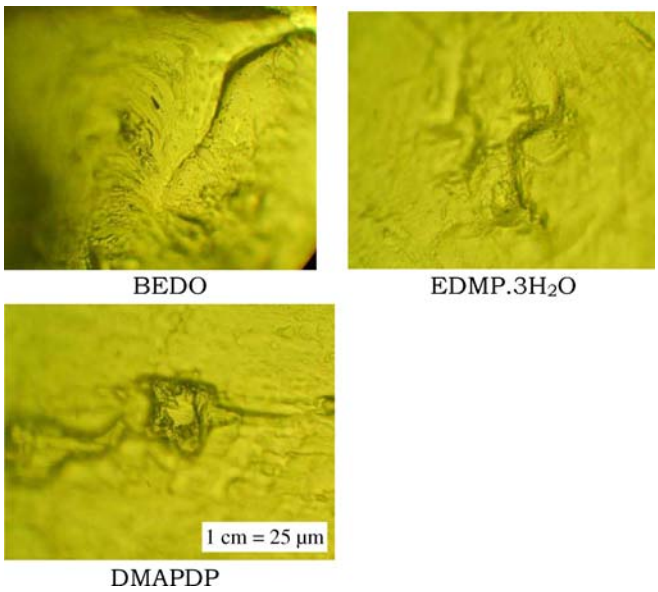


**FIGURE 8** Optical micrograph of laser induced damage (400 ×) viewed along the axis of the laser radiation

erties, were also determined. This is accomplished by measuring the intensity of the transmitted/reflected beam from the crystal when the damage actually occurred. The calculated surface damage threshold values are given in Table 1. From Table 1, it can be seen that the pure organic crystals (EMPO, BEDO, EDMP · 3 $H_2O$, MDMP · 3 $H_2O$ and DMAPT · 2 $H_2O$) have a relatively high surface damage threshold and the addition of inorganic elements (chloride and bromide) in the *N*-alkyl-2,6-dimethyl-4(1H)-pyridinone derivatives reduce the damage resistance except for MDMPBr · $H_2O$. The organic salt DMAPT · 2 $H_2O$ shows the highest damage threshold value among all the crystals reported here. A direct comparison of results with the literature values could not be made as the testing conditions, such as, wavelength and pulse widths are different. However, it can easily be seen that longer pulses prevent any thermal relaxation, thereby reducing the damage resistance. A comparison of the laser induced damage threshold values for various NLO crystals is presented in Table 1 [29–31].

Figures 6–8 show the magnified images of the damaged surface of the crystals. The morphology of the damaged patterns reveals the nature of damage and their possible origins [32]. When the damage is caused by the dielectric breakdown, there will be a clear symmetry of the resultant pattern. At the same time, when the damage is predominantly by thermal decomposition, the patterns observed do not show any symmetry and are surrounded by a circular halo. However, these are only indicative of the dominant mechanisms and the actual process of laser damage is a complex interplay of various contributing mechanisms. The dominating factor depends on various other factors like experimental geometry, specific properties of the material under investigation, pulse width and wavelength of the laser radiation used. It has been well established that in the long-pulse regime ($\tau > 100$ ps), the damage process is controlled by the rate of thermal conduction through the atomic lattice and in the short-pulse regime ($\tau < 10$ ps), the optical breakdown is a non-thermal process, and various nonlinear ionization mechanisms (such as multi-photon processes, avalanche multiplication and tunneling) become important [33]. Hence, the thermal effects become dominant for the pulse widths that are in nanoseconds as in the present case [34]. Since the investigated crystals have values of $\alpha$ which are in the range from $\sim 17$ to $34 \times 10^{-7}$ $m^2s^{-1}$ (Table 3) and the melting point ranges from $\sim 70$ to 160 °C [13, 14, 19–25], it is expected that the laser induced damage is of thermal origin.

| Crystal | Vicker's microhardness (Hv) |
|---|---|
| EMPO | 7.21 |
| BEDO | 6.57 |
| EDMP · $3H_2O$ | 31.70 |
| MDMP · $3H_2O$ | 18.00 |
| EDMPCl · $2H_2O$ | 32.80 |
| EDMPBr · $2H_2O$ | 37.20 |
| MDMPCl · $H_2O$ | 34.40 |
| MDMPBr · $2H_2O$ | 31.60 |
| DMAPDP | 45.30 |
| DMAPCl · $2H_2O$ | 42.50 |
| DMAPT · $2H_2O$ | 50.20 |
| 2A5NPFB | 68.10 |
| 2A5NPF | 34.90 |
| Literature | |
| KDP | 122–183 [17] |
| CLBO | 140–170 [35] |
| KB5 | 49–82 [36, 37] |
| L-PCA | 33 [38] |
| L-*N*-(5-Nitro-2-pyridyl) leucinol (NPLO) | 18 [39] |
| Thienylchalcone (T-17) | 17 [40] |

**TABLE 2** Vicker's microhardness of the grown crystals

From the magnified images of EMPO, EDMPCl · 2 $H_2O$, EDMPBr · 2 $H_2O$, MDMP · 3 $H_2O$, MDMPBr · $H_2O$ and DMAPT · 2 $H_2O$, (Fig. 6) it is identified that the dominant mechanism operating in the process is thermal effects. Moreover, at fluence values slightly above the threshold, there is a thermal fusion in EMPO, MDMPBr · $H_2O$ and EDMPCl · 2 $H_2O$. Since the damage patterns do not show any clear symmetry and are often surrounded by a circular halo, the damage is predominantly by thermal decomposition. Further, the damaged patterns are unique in the sense that they are highly local, without any spreading cracks or fragmentation. The patterns of MDMPCl · $H_2O$, DMAPCl · 2 $H_2O$, 2A5NPFB and 2A5NPF (Fig. 7) reflect a similar mechanism as responsible for damage, and the major contribution is due to the thermochemical ablation. The damages of BEDO, EDMP · 3 $H_2O$ and DMAPDP (Fig. 8) are by virtue of the resultant stress released in the form of propagating cracks and fragmentations under the damaging radiation. This can be noticed from the corresponding Fig. 8, which clearly indicates that the damages are not localized and spread over the surfaces as cracks. A stronger influence of the linear absorption can be found when the heating effects are taken into account. This leads to the appearance of inhomogeneous wave mismatch, hysteresis phenomena and finally to the decrease and temperature instabilities of the conversion efficiency. Due to the existence of the disrupted layer on the crystal surface and of corresponding surface defects, the surface absorption may be several orders greater than the volume absorption. Usually due to a very low thickness of the disrupted surface layer ($< 10$ nm), it is assumed that this absorption can not affect the conversion efficiency, but it can exert the primary influence on the surface-damage threshold, as discussed above.

From Table 2, it is clear that the addition of inorganic elements (chlorine and bromine) in *N*-alkyl-2,6-dimethyl-4(1H)-pyridinones (EDMP · 3 $H_2O$ and MDMP · 3 $H_2O$) improved the hardness of the material. The pure organic crystals EMPO and BEDO exhibit distinctively low mechanical hardness due to weak chemical bonds. The 4-dimethylamino-

| Crystal (density in g/cm$^3$) | Crystal thickness ($10^{-3}$ cm) | Modulation frequency (Hz) | Thermal diffusivity $\alpha$ ($\times 10^{-7}$ m$^2$s$^{-1}$) | Thermal effusivity $e$ (J m$^{-2}$K$^{-1}$s$^{-1/2}$) | Heat capacity $C_p$ (J kg$^{-1}$K$^{-1}$) | Thermal conductivity $K$ (W m$^{-1}$K$^{-1}$) |
|---|---|---|---|---|---|---|
| EMPO | 79.5 | 65 | 27.73 | 660.1 | 443.0 | 1.099 |
| (1.249) | | 70 | 28.71 | 662.0 | 436.6 | 1.122 |
| | | 75 | 29.96 | 663.1 | 428.1 | 1.148 |
| BEDO | 84.1 | 65 | 31.31 | 669.8 | 322.2 | 1.185 |
| (1.093) | | 70 | 32.27 | 670.7 | 317.8 | 1.205 |
| | | 75 | 33.56 | 670.9 | 311.7 | 1.229 |
| EDMP · $3H_2O$ | 64.3 | 65 | 17.44 | 661.4 | 716.1 | 0.873 |
| (1.207) | | 70 | 17.91 | 662.8 | 715.1 | 0.897 |
| MDMP · $3H_2O$ | 63.4 | 70 | 18.04 | 663.6 | 706.4 | 0.891 |
| (1.206) | | 75 | 18.80 | 664.8 | 693.3 | 0.911 |
| DMAPDP | 89.6 | 65 | 29.51 | 663.7 | 332.8 | 1.140 |
| (1.491) | | 70 | 30.58 | 665.9 | 328.0 | 1.164 |
| | | 75 | 31.75 | 667.2 | 322.5 | 1.189 |
| Literature [29, 30, 41–51] | | | | | | |
| KDP | | | | | 857 (298 K) | 1.21 (302 K) |
| ADP | | | | | 1236 (298 K) | 0.71, 1.26 (315 K) |
| KN | | | | | 767 | 4, > 3.5 |
| LT | | | | | 426 (300 K) | 5 (300 K) |
| Barium titanate (BT) | | | | | 439 (300 K) | 1.34 (293 K) |
| GaAs | | | | | 318 (273 K) | 52, 52.3 (300 K) |
| Bismuth triborate (BIBO) | | | | | 500 (323 K) | – |
| Yttrium calcium oxyborate (YCOB) | | | | | 729.7 (373 K) | 2.6, 2.33 (293 K) |
| Cadmium mercury thiocyanate (CMTC) | | | | | 758.8 (293 K) | – |
| Lithium thioindate (LIS) | | | | | 500 (300 K) | 6.2, 6, 7.6 |
| BBO | | | | | 490, 496 (298 K) | 1.6, 1.2 |
| LBO | | | | | 1060 (298 K) | 3.5 |
| LN | | | | | 648 (300 K) | 4.4, 4.5 (300 K) |
| KTP | | | | | 688 (298 K) | 2, 3, 3.3 |
| AGS | | | | | 404 (292 K) | 1.4, 1.5 (293 K) |
| AGSe | | | | | 297 (300 K) | 1.0, 1.1 (293 K) |
| Zinc germanium phosphide (ZGP) | | | | | 392, 464 | 36, 35 (293 K) |
| LI | | | | | 365, 569 | 0.65, 1.27 (300 K) |
| $\alpha$-$SiO_2$ | | | | | – | 11.7, 6.5 (293 K) |

**TABLE 3** Comparison of thermal parameters of the grown crystals with literature values

pyridinium salts namely DMAPDP, DMAPCl · 2 $H_2O$ and DMAPT · 2 $H_2O$ offer moderate resistance to deformation. However, the semiorganic 2A5NPFB possesses the highest hardness value as 68.10 among the investigated crystals. This is due to the high electron affinity of fluorine, tight packing of molecules in the unit cell and strong intermolecular interactions as evidenced from the crystal structure [14]. The lower hardness value can be attributed to the presence of relatively weak bonds in the molecules. Another manifestation of these weak bonds is the lower melting point, when compared with the pure inorganic materials like KDP, ADP, KTP, etc.. For the sake of comparison, the Vicker's hardness numbers (Hv) for a few NLO crystals taken from literature are listed in Table 2. The Hv values of investigated crystals are comparable with those of KB5 and L-PCA, but less than KDP.

From Table 3, it can be seen that the heat capacity of EDMP · 3 $H_2O$ is higher than those of other crystals. The thermal conductivity of EMPO, BEDO and DMAPDP are more or less the same, but higher than that of EDMP · 3 $H_2O$ and MDMP · 3 $H_2O$. Compared to the inorganic crystals, the thermal properties of organic crystals are very limited in literature and so the comparison could be made with a few known NLO crystals only. From Table 3 it can be seen that the values of $C_p$ are comparable with those of LT, BT, GaAs, YCOB, CMTC, LIS, BBO, LN, KTP, AGS, AGSe, ZGP and LI in which the $C_p$ values are in the range (297–750 J $kg^{-1}K^{-1}$). Further, the values of K in Table 3 are comparable with the other known inorganic NLO materials like KDP, ADP, BBO, AGS, AGSe and LI.

## 4 Conclusion

Our investigations on the device related properties of the grown crystals reveal that the organic crystal DMAPT · 2 $H_2O$ has a higher laser damage threshold than semiorganic crystals. The introduction of hydrogen bonds during formation of halogenides in the *N*-alkyl-2,6-dimethyl-4(1H)-pyridinones reduce the optical stability, but, increase the mechanical hardness. The unit cell packing density and strong cation and anion interactions in the herringbone structure of the semiorganic 2A5NPFB offers mechanical strength essential for crystal processing. The surface analysis of the damaged crystals illustrate the nature of damage from which the dominant mechanism operating is identified as thermal effects for the nanosecond laser with a lower repetition rate (1 Hz).

**ACKNOWLEDGEMENTS** The authors thank Dr. D. Sastikumar (Department of Physics, National Institute of Technology, Tiruchirappalli) for the facility to measure microhardness. The authors are grateful to Dr. K.C. Rustagi, Dr. S.C. Mehendale and Dr. Mukesh Joshi (Laser Physics Applications Division, Raja Ramanna Centre for Advanced Technology, Indore) for their interest in this work. SAIF, Kochi is gratefully acknowledged for the DSC. One of the authors (S.M.) is thankful to CSIR, New Delhi for the award of an SRF (File No.9/475(120)/2004-EMR-I dated 28/6/2004).

## REFERENCES

1 G.F. Lipscomp, A.F. Garrito, R.S. Narang, J. Chem. Phys. **75**, 1509 (1981)
2 J.C. Banmert, R.J. Twieg, G.C. Bjorkhmd, J.A. Logan, C.W. Dirk, Appl. Phys. Lett. **51**, 1484 (1987)
3 C. Dehu, F. Meyers, J.L. Bredas, J. Am. Chem. Soc. **115**, 6198 (1993)
4 D.J. Williams, Angew. Chem. Int. Ed. Engl. **23**, 690 (1984)
5 P.N. Prasad, D.R. Ulrich, *Nonlinear Optical and Electro Active Polymer* (Plenum, New York, 1988)
6 W. Blau, Phys. Technol. **18**, 250 (1987)
7 D. Eimerl, S. Velsko, L. Davis, F. Wang, G. Loiacono, G. Kennedy, IEEE J. Quantum Electron. **QE-25**, 179 (1989)
8 M. Jiang, Q. Fang, Adv. Mater. **11**, 1147 (1999)
9 W. Tam, B. Guerin, J.C. Calabrese, S.H. Stevenson, Chem. Phys. Lett. **154**, 93 (1989)
10 D.R. Yuan, N. Zhang, X.T. Tao, D. Xu, M.G. Liu, W.B. Hou, Y.H. Bing, M.H. Jiang, J. Cryst. Growth **166**, 545 (1996)
11 M.G. Liu, M.H. Jiang, X.T. Tao, D.R. Yuan, D. Xu, N. Zhang, Z.S. Shao, J. Mater. Sci. Lett. **13**, 146 (1994)
12 Y.L. Fur, R. Masse, M.Z. Cherkaoui, J.F. Nicoud, Z. Kristallogr. **210**, 856 (1995)
13 S. Manivannan, S. Dhanuskodi, K. Kirschbaum, S.K. Tiwari, Cryst. Growth Design **6**, 1285 (2006)
14 S. Manivannan, S. Dhanuskodi, K. Kirschbaum, S.K. Tiwari, Cryst. Growth Design **5**, 1463 (2005)
15 K. Fujioka, S. Matsuo, T. Kanabe, H. Fujita, M. Nakatsuka, J. Cryst. Growth **181**, 265 (1997)
16 S. Mukerji, T. Kar, Cryst. Res. Technol. **34**, 1323 (1999)
17 H. Yoshida, T. Jitsuno, H. Fujita, M. Nakatsuka, M. Yoshimura, T. Sasaki, K. Yoshida, Appl. Phys. B **70**, 195 (2000)
18 H. Kong, J. Wang, H. Zhang, X. Yin, S. Zhang, Y. Liu, X. Cheng, L. Gao, X. Hu, M. Jiang, J. Cryst. Growth **254**, 360 (2003)
19 S. Manivannan, S.K. Tiwari, S. Dhanuskodi, Solid State Commun. **132**, 123 (2004)
20 S. Dhanuskodi, S. Manivannan, J. Philip, J. Cryst. Growth **265**, 284 (2004)
21 S. Manivannan, S. Dhanuskodi, J. Cryst. Growth **262**, 473 (2004)
22 S. Dhanuskodi, S. Manivannan, J. Cryst. Growth **262**, 395 (2004)
23 S. Dhanuskodi, S. Manivannan, K. Kirschbaum, Spectrochim. Acta A **64**, 504 (2006)
24 S. Manivannan, S. Dhanuskodi, Cryst. Growth Design **4**, 845 (2004)
25 S. Dhanuskodi, S. Manivannan, K. Kirschbaum, J. Philip, S. Selladurai, J. Cryst. Growth **290**, 548 (2006)
26 H. Nakatani, W.R. Bosenberg, L.K. Cheng, C.L. Tang, Appl. Phys. Lett. **53**, 2587 (1988)
27 J. Swain, S. Stokowski, D. Milam, F. Rainer, Appl. Phys. Lett. **40**, 350 (1982)
28 C. Preethy Menon, J. Philip, Meas. Sci. Technol. **11**, 1744 (2000)
29 D.N. Nikogosyan, *Nonlinear Optical Crystals: A Complete Survey* (Springer, New York, 2005)
30 V.G. Dmitriev, G.G. Gurzadyan, D.N. Nikogosyan, *Handbook of Nonlinear Optical Crystals* (Springer, Berlin, 1999), 3rd edn.
31 V. Venkataramanan, C.K. Subramanian, H.L. Bhat, J. Appl. Phys. **77**, 6049 (1995)
32 B.C. Stuart, M.D. Feit, A.M. Rubenchik, B.W. Shore, M.D. Perry, Phys. Rev. Lett. **74**, 2248 (1995)
33 S.S. Gupte, R.D. Pradhan, A. Marcano O, N. Melikechi, C.F. Desai, J. Appl. Phys. **91**, 3125 (2002)
34 K.G. Subhadra, K. Kishan Rao, D.B. Sirdeshmukh, Bull. Mater. Sci. **23**, 147 (2000)
35 Y. Mori, I. Kuroda, S. Nakajima, T. Sasaki, S. Nakai, J. Cryst. Growth **156**, 307 (1995)
36 K. Thamizharasan, S. Xavier Jesu Raja, F.P. Xavier, P. Sagayaraj, J. Cryst. Growth **218**, 323 (2000)
37 S.A. Rajasekar, K. Thamizharasan, A. Joseph Arul Pragasam, J. Pakiam Julius, P. Sagayaraj, J. Cryst. Growth **247**, 199 (2003)
38 M. Kitazawa, R. Higuchi, M. Takahashi, T. Wada, H. Sasabe, Appl. Phys. Lett. **64**, 2477 (1994)
39 T. Ukachi, T. Shigemoto, H. Komatsu, T. Sugiyama, J. Opt. Soc. Am. B **10**, 1372 (1993)
40 Y. Kitaoka, T. Sasaki, S. Nakai, Y. Goto, Appl. Phys. Lett. **59**, 9 (1991)
41 L.E. Busse, L. Goldberg, M.R. Surette, G. Mizell, J. Appl. Phys. **75**, 1102 (1994)
42 Y. Uematsu, T. Fukuda, Japan. J. Appl. Phys. **12**, 841 (1973)
43 P. Blau, S. Pearl, A. Englander. A. Bruner, D. Eger, Proc. SPIE **4972**, 34 (2003)
44 B. Teng. J. Wang, Z. Wang, X. Hu, H. Jiang, H. Liu, X. Cheng, S. Dong, Y. Liu, Z. Shao, J. Cryst. Growth **233**, 282 (2001)
45 J. Luo, S.J. Fan, H.Q. Xie, K.C. Xiao, S.X. Qian, Z.W. Zhong, G.X. Qiang, R.Y. Sun, J.Y. Xu, Cryst. Res. Technol. **36**, 1215 (2001)

46 Q. Ye, L. Shah, J. Eichenholz, D. Hammons, R. Peale, M. Richardson, A. Chin, B.H.T. Chai, Opt. Commun. **164**, 33 (1999)
47 D.R. Yuan, D. Xu, G.H. Zhang, M.G. Liu, S.Y. Guo, F.Q. Meng, M.K. Lu, Q. Fang, M.H. Jiang, Chin. Phys. Lett. **17**, 669 (2000)
48 S. Fossier, S. Salaun. J. Mangin. O. Bidault, I. Thenot, J.J. Zondy, W. Chen, F. Rotermund, V. Petrov, P. Petrov, J. Henningsen. A. Yelisseyev, L. Isaenko. S. Lobanov, O. Balachninaite, G. Slekys, V. Sirutkaitis, J. Opt. Soc. Am. B **21**, 1981 (2004)
49 A. Douillet, J.J. Zondy, A. Yelisseyev, S. Lobanov, L. Isaenko, J. Opt. Soc. Am. B **16**, 1481 (1999)
50 J.D. Beasley, Appl. Opt. **33**, 1000 (1994)
51 J.E. Tucker, C.L. Marquardt, S.R. Bowman, B.J. Feldman, Appl. Opt. **34**, 2678 (1995)